Department of Applied Mechanics

Resonance phenomena of polymer-covered cylinders under rolling contact

Anssi Karttunen

Aalto University

DOCTORAL DISSERTATIONS

Aalto University publication series
DOCTORAL DISSERTATIONS 179/2015

Resonance phenomena of polymer-covered cylinders under rolling contact

Anssi Karttunen

A doctoral dissertation completed for the degree of Doctor of Science (Technology) to be defended, with the permission of the Aalto University School of Engineering, at a public examination held in lecture hall U8 on 15 December 2015 at 12.

Aalto University
School of Engineering
Department of Applied Mechanics
Mechanics of Materials

Supervising professor
Prof. Jukka Tuhkuri

Thesis advisor
Prof. Raimo von Hertzen

Preliminary examiners
Prof. Andrei Metrikine, Delft University of Technology, Netherlands
Prof. Atsuo Sueoka, Kyushu Polytechnic College, Japan

Opponents
Prof. Andrei Metrikine, Delft University of Technology, Netherlands
Prof. Aki Mikkola, Lappeenranta University of Technology, Finland

Aalto University publication series
DOCTORAL DISSERTATIONS 179/2015

ISBN 978-952-60-6501-4 (printed)
ISBN 978-952-60-6502-1 (pdf)
ISSN-L 1799-4934
ISSN 1799-4934 (printed)
ISSN 1799-4942 (pdf)
http://urn.fi/URN:ISBN:978-952-60-6502-1

Unigrafia Oy
Helsinki 2015

Finland

Aalto University

Abstract

Aalto University, P.O. Box 11000, FI-00076 Aalto www.aalto.fi

Author
Anssi Karttunen

Name of the doctoral dissertation
Resonance phenomena of polymer-covered cylinders under rolling contact

Publisher School of Engineering

Unit Department of Applied Mechanics

Series Aalto University publication series DOCTORAL DISSERTATIONS 179/2015

Field of research Mechanics of Materials

Manuscript submitted 14 September 2015 **Date of the defence** 15 December 2015

Permission to publish granted (date) 26 October 2015 **Language** English

☐ **Monograph** ☒ **Article dissertation (summary + original articles)**

Abstract

In paper machines the paper is fed through the contact areas, the nips, between rolling cylinders which are often covered with polymers. A soft polymer nip gives the paper a glossy surface and a smooth thickness profile with uniform density. Although the use polymer covers is beneficial in terms of end-product quality, the covers also induce and suffer from harmful dynamic phenomena. In this dissertation two such phenomena, a self-excited vibration mechanism and a traveling wave phenomenon, were studied in detail to understand their essential features. At all instances, the studied system consisted of two steel-core cylinders with a polymeric cover on the other cylinder.

The self-excited vibration mechanism was first investigated using a one-dimensional (1D) analytical model. It was found that the mechanism is active when the frequency of the cover deformation induced excitation is close to that eigenfrequency of the system, which corresponds to the eigenmode in which the cylinders are vibrating in opposite phases. The vibrations are strongest when the phase of the residual deformation of the cover leads the phase of the nip gap between the cylinders by 90 degrees. Next, simulations were performed using a two-dimensional (2D) plane strain finite element (FE) model and cover deformation patterns were obtained. The results from the 1D and 2D models were found to be in good agreement. Finally, the computational and obtained experimental results were compared to validate the model-based physical interpretations. The physical explanation given by the 1D analytical model for the self-excited vibration mechanism was found to be valid.

The traveling wave phenomenon was first studied using a 2D plane strain FE model. A critical speed below which the traveling waves did not appear was calculated on the basis of a resonance condition using modal information from eigenmode analysis. After dynamic rolling contact simulations it was found that the traveling wave phenomenon is best described as a Rayleigh wave resonance in which contact-induced modified Rayleigh waves arise in the nip at critical and supercritical rolling speeds and the waves superpose to form a strong traveling wave. Next, a 1D analytical cover model was developed for an elastic cylinder cover with damping. It was found that the 1D model captures the essential features of the traveling wave phenomenon. The 1D model was developed further so that the cover material was described as a frequency-dependent viscoelastic polymer. The viscoelastic model offers a simple tool for calculating estimates for the critical speeds of polymer covers in industrial use.

Keywords vibration, wave propagation, resonance, polymer, viscoelasticity, contact

ISBN (printed) 978-952-60-6501-4 **ISBN (pdf)** 978-952-60-6502-1

ISSN-L 1799-4934 **ISSN (printed)** 1799-4934 **ISSN (pdf)** 1799-4942

Location of publisher Helsinki **Location of printing** Helsinki **Year** 2015

Pages 104 **urn** http://urn.fi/URN:ISBN:978-952-60-6502-1

Aalto-yliopisto

Tiivistelmä

Aalto-yliopisto, PL 11000, 00076 Aalto www.aalto.fi

Tekijä
Anssi Karttunen

Väitöskirjan nimi
Polymeeripinnoitettujen pyörivien kontaktitelojen resonanssi-ilmiöt

Julkaisija Insinööritieteiden korkeakoulu

Yksikkö Sovelletun mekaniikan laitos

Sarja Aalto University publication series DOCTORAL DISSERTATIONS 179/2015

Tutkimusala Lujuusoppi

Käsikirjoituksen pvm 14.09.2015 **Väitöspäivä** 15.12.2015

Julkaisuluvan myöntämispäivä 26.10.2015 **Kieli** Englanti

☐ **Monografia** ☒ **Yhdistelmäväitöskirja (yhteenveto-osa + erillisartikkelit)**

Tiivistelmä

Paperikoneissa paperi kulkee pyörivien telojen kontaktialueiden eli nippien läpi. Telat on usein päällystetty polymeereillä. Pehmeä polymeerinippi antaa paperille kiiltävän pinnan sekä tasaisen paksuusprofiilin ja tiheysjakauman. Vaikka polymeeripinnoitteiden käyttäminen onkin hyödyllistä lopputuotteen laadun kannalta, pinnoitteet kärsivät myös haitallisista dynaamisista ilmiöistä. Tässä väitöskirjassa tutkittiin kahta tällaista ilmiöitä – itseherätteistä värähtelymekanismia ja etenevää aaltoilmiötä. Työn tarkoituksena oli selvittää näiden ilmiöiden keskeiset piirteet. Kaikissa tutkimuksen vaiheissa tutkittava telasysteemi koostui kahdesta pyörivästä telasta ja toinen tela oli päällystetty polymeeripinnoitteella.

Itseherätteistä värähtelymekanismia tarkasteltiin ensin käyttäen yksiulotteista analyyttista mallia. Tutkimuksessa selvisi, että värähtelymekanismi on aktiivinen, kun pinnoitteen aiheuttaman pakkoherätteen ominaistaajuus on lähes sama kuin ominaistaajuus, joka vastaa ominaismuotoa, jossa telat värähtelevät vastakkaisissa vaiheissa. Värähtelyt ovat voimakkaimmillaan, kun pinnoitteen jäännösmuodonmuutoksen vaihe on 90 astetta nippiraon vaihetta edellä. Seuraavaksi värähtelyitä tutkittiin käyttäen kaksiulotteista tasovenymäelementtimallia, jonka avulla mallinnettiin värähtelymekanismin aiheuttamia telapinnoitemuodonmuutoksia. Tutkimuksen viimeisessä vaiheessa yksi- ja kaksiulotteisia laskennallisia tuloksia ja kokeellisia tuloksia verrattiin toisiinsa laskennallisten mallien ja niiden perusteella muodostettujen fysikaalisten tulkintojen vahvistamiseksi.

Etenevää aaltoilmiötä tutkittiin ensin käyttäen kaksiulotteista elementtimallia tasovenymätilassa. Ominaismuotoanalyysin tulosten perusteella telapinnoitteelle laskettiin kriittinen nopeus, jonka alapuolella etenevät aallot eivät ilmesty telapinnoitteeseen. Dynaamisten kontaktisimulaatioiden jälkeen todettiin, että etenevää aaltoilmiöitä on parasta käsitellä Rayleigh-aaltoresonanssina, jossa telakontaktin aiheuttamat modifioidut Rayleigh-aallot syntyvät nipissä sekä kriittisillä että ylikriittisillä nopeuksilla ja summautuvat voimakkaaksi eteneväksi aalloksi. Seuraavaksi aaltoilmiöitä kuvaamaan kehitettiin yksiulotteinen malli vaimennetulle elastiselle telapinnoitteelle. Vertailemalla keskenään yksi- ja kaksiulotteisista malleista laskettuja tuloksia todettiin, että yksiulotteinen malli kuvaa hyvin etenevän aaltoilmiön keskeisimmät ominaisuudet. Mallia jatkokehitettiin siten, että pinnoitemateriaali kuvattiin taajuusriippuvaisena viskoelastisena aineena. Näin ollen mallilla voidaan helposti laskea teollisuudessa käytettävien telapinnoitteiden kriittiset nopeudet.

Avainsanat värähtely, etenevä aalto, resonanssi, polymeeri, viskoelastisuus, kontakti

ISBN (painettu) 978-952-60-6501-4 **ISBN (pdf)** 978-952-60-6502-1

ISSN-L 1799-4934 **ISSN (painettu)** 1799-4934 **ISSN (pdf)** 1799-4942

Julkaisupaikka Helsinki **Painopaikka** Helsinki **Vuosi** 2015

Sivumäärä 104 **urn** http://urn.fi/URN:ISBN:978-952-60-6502-1

Preface

This dissertation and the related journal papers were written during the years 2010–2014 in the Solid Mechanics group at the Department of Applied Mechanics at Aalto University. In the course of my doctoral studies I have been funded by the Ministry of Education and Culture of Finland through the National Graduate School in Engineering Mechanics and by Aalto University School of Engineering. I gratefully acknowledge this financial support.

I would like to express my sincere gratitude to my advisor, Professor Raimo von Hertzen, for all his support and our countless discussions during the past years. I am thankful to my supervisor, Professor Jukka Tuhkuri, for his encouragement and the provided exemplary working conditions. It has been an honour and a privilege to have Professors Atsuo Sueoka and Andrei Metrikine as the preliminary examiners of this thesis. My compliments also go to everyone in the Solid Mechanics group for their assistance and kindness.

My friends here, there and everywhere deserve the highest of fives for all the good times. With the benefit of hindsight, I find it easy to say that it is the new people you meet and become friends with during your studies who really make the road worth traveling. Remember to stay *loose*.

Finally, I want to thank my whole family for all their love and support during my studies and throughout my life.

Otaniemi, October 28, 2015,

Anssi Karttunen

Contents

List of Publications

This thesis consists of an overview and of the following publications which are referred to in the text by their Roman numerals.

I Anssi T. Karttunen and Raimo von Hertzen. Polymer cover induced self-excited vibrations of nipped rolls. *Journal of Sound and Vibration*, 330, 3959–3972, 2011.

II Anssi T. Karttunen and Raimo von Hertzen. On the self-excited vibrations of a viscoelastically covered cylinder in rolling contact using FE method. *Journal of Structural Mechanics – Special issue for NSCM-24*, 44, 231–242, 2011.

III Anssi T. Karttunen and Raimo von Hertzen. A numerical study of traveling waves in a viscoelastic cylinder cover under rolling contact. *International Journal of Mechanical Sciences*, 66, 180–191, 2013.

IV Anssi T. Karttunen and Raimo von Hertzen. Dynamic response of a cylinder cover under a moving load. *International Journal of Mechanical Sciences*, 82, 170–178, 2014.

Author's Contribution

Publication I: "Polymer cover induced self-excited vibrations of nipped rolls"

- Anssi Karttunen (AK) developed the 1D analytical model together with Raimo von Hertzen (RvH).
- AK did all the numerical calculations and analyzed them with RvH.
- AK did the experiment in collaboration with an industrial company.
- AK wrote the paper. RvH contributed to the paper with valuable comments and suggestions.

Publication II: "On the self-excited vibrations of a viscoelastically covered cylinder in rolling contact using FE method"

- AK developed the 2D FE model and did all the numerical simulations.
- AK wrote the paper. RvH contributed to the paper by giving valuable comments and suggestions.

Publication III: "A numerical study of traveling waves in a viscoelastic cylinder cover under rolling contact"

- AK developed the 2D FE model and did all the numerical simulations, which were discussed broadly along the way with RvH.
- AK wrote the paper, which RvH commented extensively during the writing process.

Publication IV: "Dynamic response of a cylinder cover under a moving load"

- AK developed and analyzed the 1D model together with RvH.
- AK did all the numerical calculations.
- AK wrote the article with welcomed oversight and assistance from RvH.

1. Introduction

The paper used for this dissertation has gone through a soft calender.

1.1 Motivation

The old proverb tells us that “Finland lives from the forest”. While this was the slogan of the Finnish paper industry still in the 1980s, times have changed and quite a few paper mills have been closed down in Finland since those days under pressure from global competition. However, in spite of the decline, the impact of forest and paper on the Finnish economy remains significant. Currently, forestry and the forest industry make up about 5% of Finland’s gross domestic product and 20% of Finnish exports (METLA, 2014). Interestingly, high-quality printing and writing paper make up over 40% of the total export value of forest industry products.

In papermaking, the finishing of the surface properties of a high-quality product consists of several stages such as sizing, coating and calendering. In these processes, the paper runs through the contact areas, the nips, between rolling steel-core cylinders. A two-cylinder system is presented schematically in Fig. 1.1 as a representative example. As is often the case, the other cylinder is covered with a polymer layer to widen the nip between the cylinders which leads to a more evenly distributed compression in the nip. Running the paper through a soft polymer nip gives the paper a glossy surface and a smooth thickness profile with uniform density. On the other hand, a wider nip allows a longer manipulation time of the paper sheet and, consequently, enables a higher production speed. Due to the benefits of polymeric cylinder cover materials, their development has been rapid since the 1990s and their use in paper machines has become commonplace.

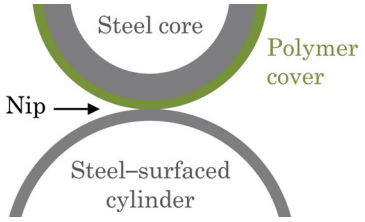

Figure 1.1. Two-cylinder system, for example, a soft calender, with a polymer cover on the upper cylinder. The cover is "soft" in comparison to the steel parts.

In contrast to their many virtues, the polymer covers also induce and suffer from detrimental dynamic phenomena, which have not been fully explained yet, let alone dealt with. Two prime examples of such phenomena are: 1) the self-excited vibration mechanism, barring, which is caused by viscoelastic cover deformations acting as time-delayed feedbacks in a rolling contact machine, and 2) a contact-induced traveling wave phenomenon occuring in a cover at high rolling speeds. These two are the subject of this dissertation.

It is elemental for any paper machine or papermaker company to understand the mechanical behavior of cylinder covers under rolling contact in order to keep their machines and mills running – under pressure from global competition.

1.2 Objectives

This work focuses on the dynamics of a polymer-covered cylinder under rolling contact. At all times, it is assumed that the cover consists of a single-layer of a polymer attached to a rigid circular core. The covered cylinder rolls in contact with a rigid-surfaced cylinder. The paper sheet is not modeled. Our aim is to, under the foregoing assumptions, provide comprehensive understanding of the two above-mentioned dynamic phenomena. In more detail, the two main objectives of this work are:

- To provide a thorough explanation of the cover-induced self-excited vibration mechanism (barring) by linking it in a clear manner to a resonance condition of a two-cylinder rolling contact system.
- To look at the contact-induced traveling wave phenomenon in a cylinder cover from both vibration and wave propagation perspectives to form a uniform, exhaustive description of its essential features.

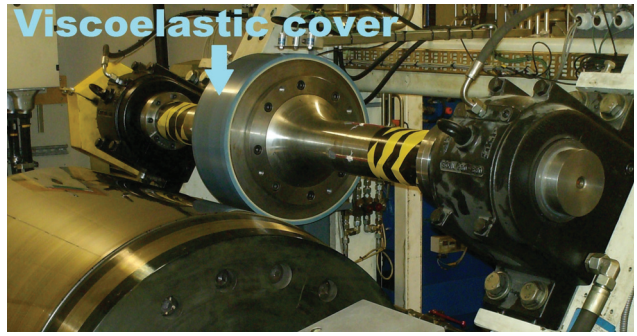

Figure 1.2. Two-cylinder testing machine with a polymer cover on the upper cylinder. The diameter of the upper cylinder's steel core is 41 cm.

1.3 Outline

Chapters 2 and 3 of this work begin with descriptions of the self-excited vibration mechanism and traveling waves, respectively, and provide surveys on the related literature, followed by principal theoretical and computational developments and results. Chapter 4 summarizes the work.

The emphasis of this dissertation is on theoretical and computational modeling of a two-cylinder rolling contact machine to achieve fundamental understanding of the two phenomena at hand. All developed models are based on an industrial rolling contact testing machine presented in Fig. 1.2. The machine has been built by a paper machine company to study the effect of the self-excited vibrations on different polymer covers. The parameter values used in computations are obtained from the testing machine and polymer covers in industrial use.

The self-excited vibration mechanism is first investigated using a one-dimensional (1D) analytical model, which yields a set of delay differential equations to be studied through numerical stability analysis (**PI**). Then, simulations are performed using a two-dimensional (2D) plane strain finite element (FE) model (**PII**). Finally, computational and experimental results are compared to validate model-based physical interpretations.

The traveling wave phenomenon is studied first by the aid of a 2D plane strain FE model (**PIII**). After acquiring a clear picture of the key features of the traveling waves via 2D numerical experimentation, a 1D analytical cover model is developed, which is amenable to a detailed theoretical study in the case of an elastic cylinder cover (**PIV**). As the last item, the 1D model is modified slightly for industrial purposes by describing the cylinder cover material as a frequency-dependent viscoelastic polymer that spans a wide relaxation spectrum.

2. Self-excited vibrations

In papermaking, when a paper sheet is calendered using a two-cylinder assembly with a polymer cover on the other cylinder, the cover deforms to an out-of-round shape in the nip. The viscoelastic cover deformations recover, for the most part, quite rapidly outside the nip. However, what remains after one revolution period, is fed back into the nip. This time-delayed feedback causes the cylinders to vibrate, which in turn can lead to the formation of a periodic polygonal deformation pattern in the polymer cover, see Fig. 2.1. Furthermore, the wave-like surface pattern may grow gradually, which can be observed as severe vibration of the calender during its operation. Ultimately, this self-excited vibration results in defective products making the continuous operation of the calender impossible. The vibration caused by the deformation pattern, which presents itself to the eye as stripes or bars in the axial direction of the covered cylinder, is often referred to as barring vibration. In this chapter, we study this cover-induced self-excited vibration mechanism in a two-cylinder system.

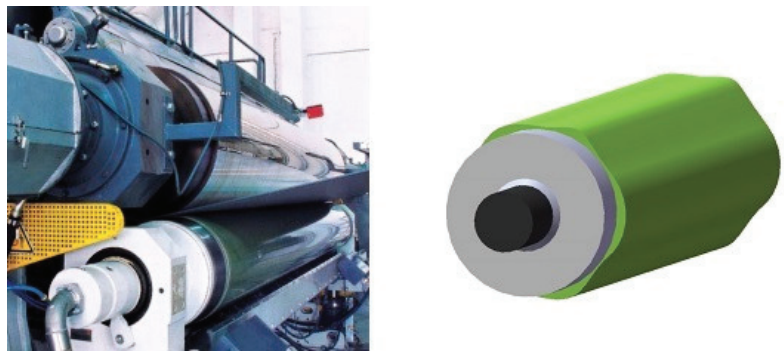

Figure 2.1. Soft-calender and a wave-like polygonal deformation pattern of the polymer cover of the lower cylinder. The deformations have been exaggerated for illustrative purposes. Commonly they are of the order of several, or even a few tens, of micrometres.

2.1 Overview of literature

Sueoka et al. (1996) have studied both experimentally and theoretically the problem at hand, which consists of two interconnected aspects, the vibrations of an entire two-cylinder system and the mechanical behavior of the polymer cover attached to one of the cylinders. In their 1D analytical lumped-mass description of the system, the cover was modeled using a three-parameter viscoelastic Kelvin-Voigt element. Sueoka et al. (1998) have used a similar modeling approach for the winder of a textile machine. Moreover, Sowa et al. (2006) have later used same type of models, as well as Jorkama and von Hertzen (2003, 2007), who studied the self-excited vibrations in paper winding. In these winding configurations, a wound paper roll with an increasing diameter acts as the viscoelastic component of the system. Several vibration phenomena appearing in industrial paper winding machines can be identified from their results.

Yuan (2002) has also studied cover-induced self-excited vibrations comprehensively by using a 1D model. Järvenpää and Yuan (2007, 2009) have developed industrial-scale computational models to simulate the vibrations and have studied means to mitigate them. In order to model the nip behavior more accurately, Yuan and Järvenpää (2009) have used a 2D contact mechanical model in association with a 1D two-cylinder system.

Experimental studies focusing on the behavior of polymer covers under rolling contact and the effect of environmental factors therein have been conducted by Vuoristo et al. (2000, 2002); Vuoristo and Kuokkala (2002, 2004) and Vuoristo (2004). They have used short duration force pulses to simulate the actual nip loading, the duration of which is usually between 0.2–1.0 ms. Experiments in which the loading is repeated multiple times with short time intervals to study the accumulation of the viscoelastic deformations are still needed. Experimental data on barring can be found in the works of Chinn (1999) and Rautiainen et al. (2000).

Despite all earlier studies, the self-excited vibrations are still a problem and the generation mechanism of them is not yet fully understood. When it comes to two-cylinder systems, it is understood, in general, that the mechanism is related to a resonance condition of the cylinders but a clear description of the phenomenon has not been given in the literature. We set out to elucidate the self-excited vibration mechanism through numerical stability analysis of our novel 1D model and 2D FE simulations, and seek to validate our physical interpretations through an experiment.

2.2 1D analytical model

Let us consider the two-cylinder system with a polymer cover on the upper cylinder shown in Fig. 2.2. The cylinders are modeled by masses m and M. The polymer cover based on the Maxwell-type Standard Linear Solid (SLS) is massless. The displacement coordinates for the upper and lower cylinder are x and X, respectively. The cylinder supports are modeled by springs and viscous dashpots with stiffness and viscous damping coefficients k and c for the upper cylinder, and K and C for the lower one, respectively. The parameters for the SLS element are k_∞, k_1 and c_1, where the latter two form a Maxwell element. The coordinate z determines the movement of the spring's end plate in the damper of the Maxwell element.

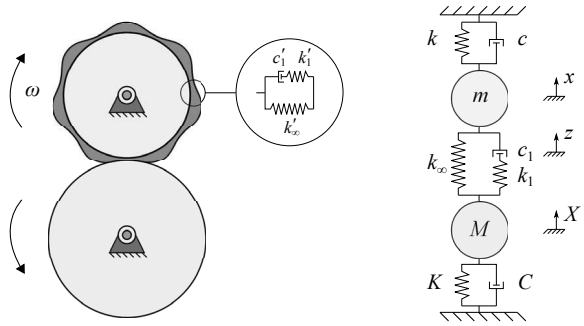

Figure 2.2. Polymer-covered two-cylinder system. In the 1D model, the cylinders are modeled as rigid bodies and the cover by an SLS element. Parameters k_1', k_∞' and c_1' refer to the configuration in which the cover recovery is studied. The values of the parameters are the same as for k_1, k_∞ and c_1, respectively.

The extensional viscous deformation of the polymer cover is defined by $\Delta l(t) = x(t) - z(t)$. When the SLS element of Fig. 2.2, attached to the upper cylinder and rotating with it, is located outside the nip we obtain from the force equilibrium of the element for the viscous deformation of the element outside the nip $\Delta l(t) = e^{A(t-t_0)}\Delta l(t_0)$, where $\Delta l(t_0)$ is the viscous deformation of the element at time t_0 when the element comes out of the nip. The recovery coefficient of the deformation is $A = -\frac{k_\infty}{k_\infty + k_1}\frac{1}{\tau_1}$ and it has an effective retarded value of $-2.9\ \mathrm{s}^{-1}$, as explained in Publication I. The relaxation time of the polymer cover is $\tau_1 = c_1/k_1 = 0.85$ ms. When the element enters the nip after one revolution at time t, it contains a non-recovered residual deformation $\Delta l(t) = e^{AT_1}\big[x(t - T_1) - z(t - T_1)\big]$, where T_1 is the length of the previous revolution period of the upper roll. In the nip, the new viscous deformation is added to the residue from the previous period. The addition is made so that the deformation from the previous

period keeps on decaying and does not simply vanish out of existence after one revolution. By generalizing this superposition principle, it can be seen that when the SLS element enters the nip, the total non-recovered viscous deformation is the sum of all contributions from preceding periods, that is,

$$\Delta l(t) = \sum_{k=1}^{N} e^{AT_k} \left[x(t - T_k) - z(t - T_k) \right] , \tag{2.1}$$

where N is the number of revolution periods of the upper roll at time t and T_k is the time for k preceding periods. The superposition is an improved part in analysis in comparison to earlier 1D models, cf. Sueoka et al. (1996). In conclusion, the use of the sum in Eq. (2.1) is a consequence of the one-dimensionality of the model and bears resemblance to the Boltzmann superposition principle in viscoelasticity (Ward and Sweeney, 2004).

The equations of motion for the system are of the form

$$\mathbf{M}\ddot{\mathbf{X}}(t) + \mathbf{C}\dot{\mathbf{X}}(t) + \mathbf{K}\mathbf{X}(t) = \mathbf{K}_1 \sum_{k=1}^{N} e^{AT_k} \mathbf{X}(t - T_k) , \tag{2.2}$$

where, $\mathbf{M}$, $\mathbf{C}$ and $\mathbf{K}$ are the mass, damping and stiffness matrices, respectively, and the displacement coordinates are $\mathbf{X} = \{x\ z\ X\}^{\mathrm{T}}$. On the right-hand side, we have the driving force due to residual deformation, which is exerted on both cylinders in the nip as an impact via the spring of the Maxwell element (note $\mathbf{K_1}$), the damper being momentarily stiff due to the lack of time to react under the load of the residual deformation entering the point-like nip. If the revolution frequencies of the cylinders are constant, we have $T_k = kT$ for the covered one.

The vibrational behavior of the system can be investigated through stability analysis by Laplace transforming Eqs. (2.2) from the time domain t to the Laplace domain s. The roots $s_i = \alpha_i + j\beta_i$ $(i = 1, 2, \ldots)$ can be solved from the resulting characteristic equation of the system. The system is unstable and exhibits strong vibrations if the real part of even one root is positive. The imaginary part of each root can be written as

$$\mathrm{Im}[s_i] = 2\pi N_i f , \tag{2.3}$$

where f is the revolution frequency of the upper cylinder and N_i is the so-called *polygonal number*. The cover deformation pattern is linked to the vibration frequency of the system – the shape of the pattern is determined by the number of vibration periods of the upper cylinder during one revolution period T. Although the system has an infinite number of the described *polygonal roots*, the study can be limited to only those roots, which correspond to deformation patterns appearing in real machines.

By neglecting the rotational motion of the cylinders, one can calculate the eigenfrequencies of the system from

$$\omega_{n,i} = \sqrt{\mathrm{Re}[s_i]^2 + \mathrm{Im}[s_i]^2}\,, \tag{2.4}$$

where $i = 1, 2$. Alternatively, the undamped eigenfrequencies can be calculated by setting $c_1 \to \infty$. This approach is often used for the sake of simplicity. However, in this case the eigenfrequencies can be misleading when analysing the self-excited vibrations.

A path of analysis not taken in the discussed literature, is to substitute the solved polygonal roots back into the Laplace-transformed equations of motions to obtain the complex eigenmodes of the system. The phase angles can be solved from the complex eigenmodes by

$$\arg(\hat{\mathcal{X}}_i) = \arctan \frac{\mathrm{Im}[\hat{\mathcal{X}}_i]}{\mathrm{Re}[\hat{\mathcal{X}}_i]}\,, \tag{2.5}$$

where $\hat{\mathcal{X}}_i = \hat{x}_i, \hat{z}_i, \hat{X}_i$ $(i = 1, 2, \ldots)$ and the "hat"-symbol is used to denote Laplace-transformed coordinates. It can be shown that, for the ith eigenmode, the phasor of the residual deformation Δl is

$$\Delta\hat{l}_i = \sum_{k=1}^{N} e^{kAT} e^{-k s_i T} (\hat{x} - \hat{z})_i\,. \tag{2.6}$$

Therefore, phase angle of the residual deformation can also be calculated. The phase angle relations of the system play a key role in understanding the self-excited vibration mechanism.

2.3 1D computational results

In the numerical analysis, a case with parameter values acquired from the machine presented in Fig. 1.2 was studied. The viscoelastic memory of the cover was taken into account from the previous period, thus $N = 1$. A larger memory affects the magnitude of the feedback force, but does not change the overall physical behavior of the system in a drastic manner.

When calculated from Eq. (2.4), the eigenfrequencies of the system are $f_{n,1} = 36.68$ Hz and $f_{n,2} = 187.3$ Hz. The corresponding (undamped) values calculated at the limit $c_1 \to \infty$ are 36.69 Hz and 193.4 Hz. In the first eigenmode of the system, the cylinders are vibrating practically in the same phase, which does not lead to self-excited vibrations. In the second eigenmode the cylinders are vibrating almost in opposite phases, causing cover deformations able to synchronize with the second eigenmode.

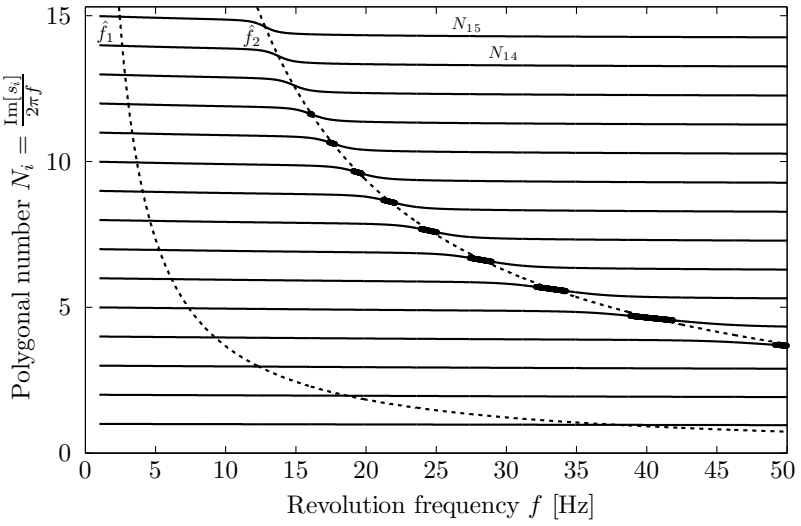

Figure 2.3. Polygonal numbers as a function of the revolution frequency of the upper cylinder. The thicker lines represent the unstable barring areas of the system. There is a barring threshold at $f = 15.8$ Hz related to the polygonal number N_{12}.

Fig. 2.3 shows, for $i = 1, 2, \ldots, 15$, the polygonal numbers N_i of the roots s_i as a function of the revolution frequency f of the upper cylinder. In addition, the unstable parts of the complex roots ($\alpha_i > 0$) are illustrated by thicker lines in the figure, and the eigenfrequencies computed from Eq. (2.4) have been presented relative to the revolution frequency, that is, $\hat{f}_1 = f_{n,1}/f$ and $\hat{f}_2 = f_{n,2}/f$.

It can be seen from Fig. 2.3 that the unstable vibrations arise when the frequency of the deformation pattern induced excitation is equal or almost equal to the higher eigenfrequency of the system, that is, $fN_i \approx f_{n,2}$. Therefore, the unstable vibration of the system is related to the resonance vibration. As representative examples, let us consider the polygonal numbers N_{10} and N_9. From the figure, one can calculate that when N_{10} (N_9) crosses curve $\hat{f}_2$, the frequency of the deformation pattern induced excitation is 19.4 Hz$\times$9.63$\approx$187 Hz (21.7 Hz$\times$8.63$\approx$187 Hz). This should be compared to the eigenfrequency $f_{n,2} = 187.3$ Hz of the non-rotating system. As mentioned earlier, using the undamped eigenfrequencies can be misleading when pondering on physical interpretations. When the polygonal numbers approach the curve $\hat{f}_2$, their values decrease steadily. The lowering non-integer polygonal number is related to the fact that when observed from the side, it seems as if the surface pattern was moving in the opposite direction relative to the cylinder's rotational motion.

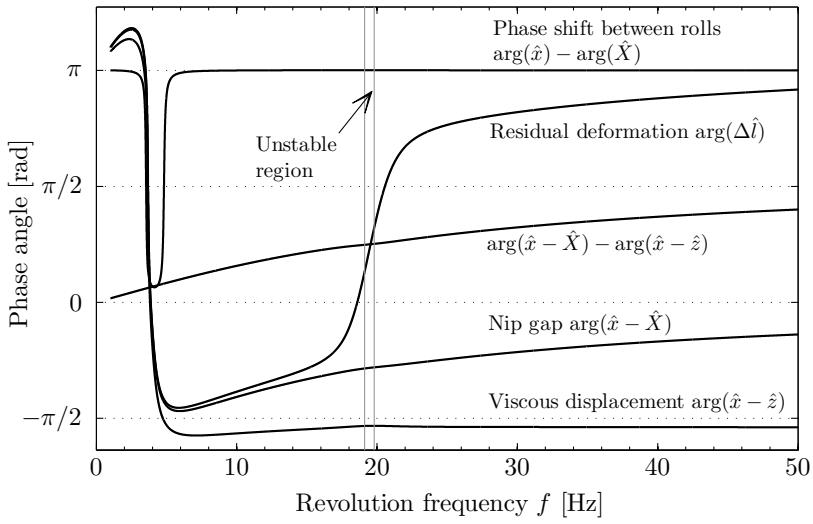

Figure 2.4. Phase angle relations of the eigenmode corresponding to the root s_{10}, which is unstable between $f = 19.1$–19.7 Hz.

Fig. 2.4 shows phase angle relations between the displacement coordinates of the system as a function of the revolution frequency of the upper cylinder for root s_{10}. It can be seen from the phase shift $\arg(\hat{x}) - \arg(\hat{X})$ between the cylinders that the polygonal shape of the cover corresponding to N_{10} keeps the system almost invariably in the higher eigenmode.

Near the unstable barring region, the phase angle $\arg(\Delta\hat{l})$ of the residual deformation has a peculiar transition zone. When the real part of the root s_{10} is at its maximum ($f = 19.4$ Hz), the phase of the residual deformation precedes the nip gap $\arg(\hat{x} - \hat{X})$ by 90 degrees. Based on this, it can be deduced that the maximum (minimum) of the residual deformation, that is, the "hill top" ("valley") of the deformation pattern, enters the nip at an instance at which the cylinders are in their equilibrium positions and their velocities are at peak values. If the cylinders are separating from each other, an elevated part on the polymer cover enters the nip to amplify the vibration. Correspondingly, if the cylinders are moving towards each other, a sunken part of the cover enters the nip. In conclusion, the phase shifts are favorable for the growth of the self-excited vibrations, and the situation corresponds to the resonance of a 1-DOF system, where the driving force precedes the displacement by 90 degrees. Beyond the unstable region, the phase shift between the residual deformation and the nip gap settles at 180 degrees. The analysis of Figs. 2.3 and 2.4 constitutes a novel, thorough explanation for the self-excited vibration mechanism.

2.4 2D vibration simulation

In this section we use a 2D plane strain FE model to obtain quantitatively realistic simulation results on a deformation pattern generated in a polymer cover. Such results are not available in the discussed literature. The system under investigation is shown in Fig. 2.5. The polymer-covered upper cylinder is rolling in frictionless contact with the lower, rigid-surfaced cylinder. The contact is created by setting a vertical force F to the center of the upper cylinder, which is supported by a linear spring-damper system. The steel core of the cylinder is modeled as rigid and the mass of the core is m. The polymer cover is linearly viscoelastic and spans a wide relaxation spectrum. The parameter values of the system are obtained from the machine of Fig. 1.2. The thickness of the polymer cover is 7 mm and it is modeled using 27160 constant strain triangle finite elements.

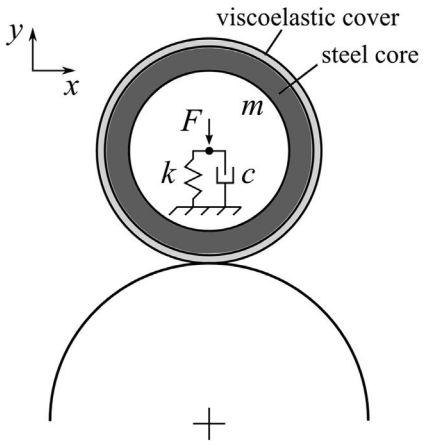

Figure 2.5. Schematic representation of the system studied using Abaqus/Explicit.

The cylinder is accelerated from rest to an angular velocity of $\omega = 100$ rad/s using a linear ramp in the time interval 0–5 s. In the interval 5–55 s, a smaller angular acceleration is applied and after 55 s the achieved angular velocity $\omega = 146.1$ rad/s ($f_r = \omega/2\pi = 23.25$ Hz) is held constant. After the contact has been created during the first two seconds, the vertical force at the center of the upper cylinder is $F = 50$ kN and the vertical displacement of the upper cylinder's centerpoint is 70 μm. The size of the contact area between the cylinders has an effect on the eigenfrequency of the system and, thus, the eigenfrequency exhibits small fluctuations under notable vibrations. With the created nip compression the eigenfrequency for the vertical vibration of the upper cylinder is $f_n = 210$ Hz at low speeds before the self-excited vibration mechanism becomes active.

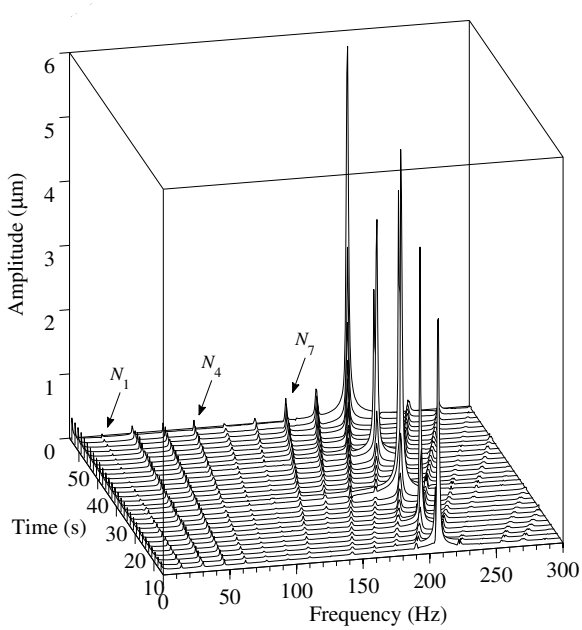

Figure 2.6. Waterfall plot computed by FFT from the displacement signal of the upper cylinder in the time interval 5–55 s. The amplitude peak appears at 210 Hz corresponding to the eigenfrequency of the system. Thus, the self-excited vibration mechanism causes the system to resonate powerfully.

Fig. 2.6 shows a waterfall plot computed using the vertical centerpoint displacement signal of the upper cylinder from the time interval 5–55 s. Fig. 2.6 shows that there are amplitude peaks in the vicinity of $f = 210$ Hz corresponding to strong vibration velocity ranges, indicating that the system is in resonance due to the self-excited vibration mechanism. Here, the polygonal numbers are defined by $N_i = f/f_r$. At $t = 60$ s, the polygonal number is $N_9 = f/f_r = 210 \,/\, 23.25 \approx 9$. It can be seen from Fig. 2.6 that the polygonal deformation patterns seem to co-exist especially near $f = 210$ Hz, however, only one is clearly dominant at a time.

In the performed simulation, the contact between the cylinders is removed at $t = 60$ s and the angular velocity is decreased to zero using a linear ramp within the time interval 60–61 s. Fig. 2.7 shows clearly that the deformation pattern generated by the vibration consists of nine sinewave-like humps. It can be seen that within the time interval 60–61 s the average radial displacement of 3.5 μm of the cover surface decreases by about 0.15 μm, while the wave-like deformation pattern itself remains practically unchanged. This shows that the wave pattern in this case is mainly due to slower relaxation processes, for which the relaxation times are clearly longer than 1 s.

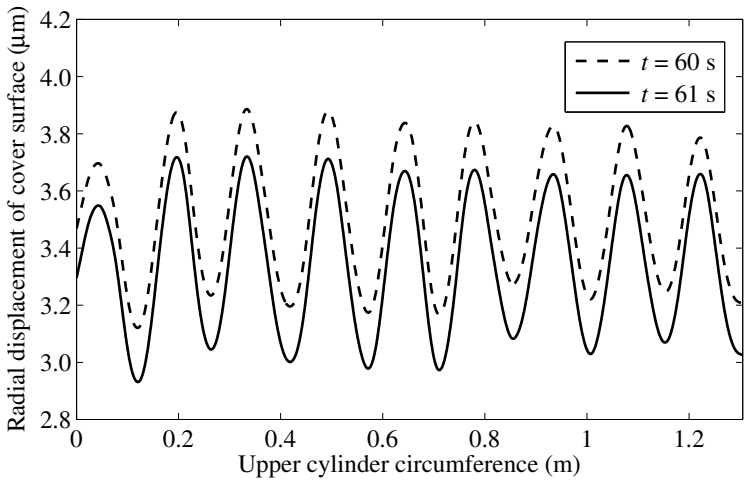

Figure 2.7. Wave-like polygonal deformation pattern in the polymer cover generated by the self-excited vibration mechanism. The relaxation of the wave–like deformation pattern is a long-term process.

A similar waterfall plot as given in Fig. 2.6 can be obtained using the 1D model and the unstable barring areas can overlap also in this case (PI). The 2D numerical experiment produces a realistic deformation pattern, the wave-like shape of which is deducible also from the 1D model. Overall, the results given by the 1D and 2D approaches are in concordance, showing no radical discrepancies. The cover bulges near the edges of the nip in the 2D model but this does not have a notable effect on the vibrational behavior of the system (see PII). Ultimately, we find that the 2D results back up the physical explanation given for the self-excited vibration mechanism by the aid of the 1D model. Let us conclude that it would be immensely difficult and computationally very expensive to form such a detailed interpretation using a 2D FE model, but a 2D computational approach may serve a practising engineer better when quantitative information on the overall system behavior is needed.

2.5 Experimental study

Finally, in order to get empirical information on the cover-induced self-excited vibrations in a rolling contact system and to understand some of the limitations imposed by the 1D and 2D modeling approaches, an experiment was carried out in Publication I using the machine presented in Fig. 1.2. The maximum rotational speed of the polymer-covered up-

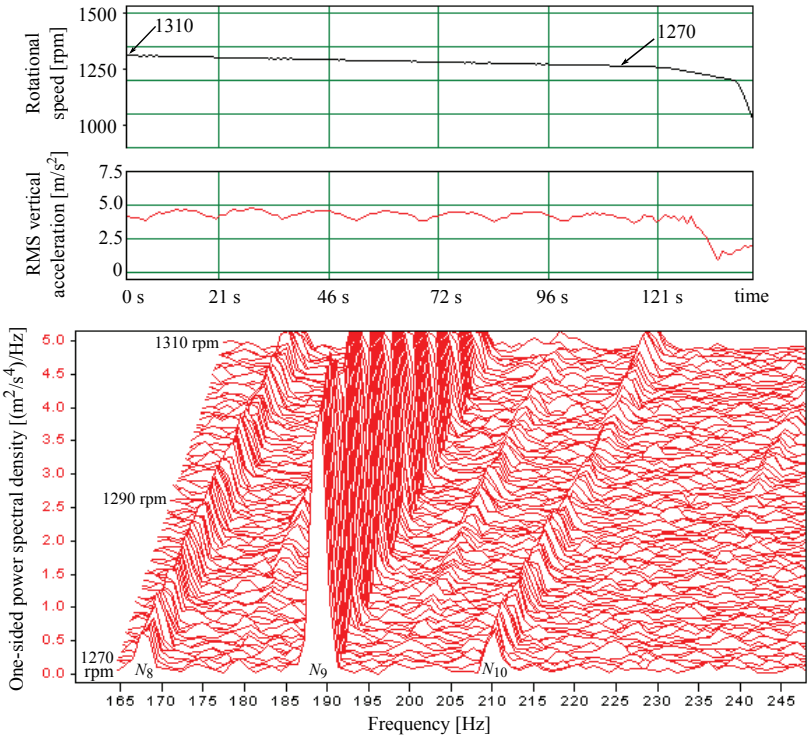

Figure 2.8. Upper part shows the rotational speed of the upper cylinder and its vibration signal, that is, the measured root-mean-square vertical acceleration. The lower part shows the real-time power spectrum as a function of time calculated from the acceleration signal between 1310...1270 rpm (0–112 s). At 1310 rpm, time has been set to zero. The polygonal numbers related to the peaks are shown in the figure.

per cylinder of the machine was 1500 rpm ($f = 25$ Hz). Only the upper cylinder was rotated by a motor while the lower cylinder rotated due to frictional forces in the nip. In the experiment, the nip was formed and the upper cylinder was accelerated to 1500 rpm in 15 minutes. From 1500 rpm, the speed was lowered quickly to 1400 rpm. Based on the 1D numerical calculations, the polygonal number N_9 should cause strong vibrations in the system between 1326...1272 rpm (22.1...21.2 Hz). The main purpose of the test was to drive slowly through this zone starting from 1400 rpm and obtain practical understanding of the occurring phenomena. Between 1400...1330 rpm the system remained stable, after which the vibration level began to rise rapidly in an exponential fashion. Fully-developed barring can be examined in Fig. 2.8. The upper part of Fig. 2.8 shows the rotational speed of the upper cylinder and its vibration signal, that is, the measured root-mean-square vertical acceleration. The lower part shows the real-time power spectrum calculated from the vibration

signal between 1310...1270 rpm (0–112 s). The cylinder contact had to be removed shortly after 1270 rpm to prevent the break-down of the polymer cover; strong vibration may be sustained only for a few minutes.

It can be seen from Fig. 2.8 that the maximum vibration acceleration is reached around the rotational speed 1300 rpm. After this, the acceleration has a lowering trend, which indicates that the vibration is weakening, which corresponds to 1D and 2D numerical results. The primary peaks in the spectrum lie in the vicinity of 190 Hz. In particular, at the rotational speeds 1310 and 1270 rpm the primary peaks lie at 194 and 189 Hz, respectively, exhibiting a lowering trend for decreasing rotational speed. If the polygonal numbers corresponding to the primary peaks are calculated by dividing the frequencies of the peaks by the corresponding revolution frequencies (21.83 and 21.17 Hz), we get 8.89 and 8.93, respectively. The result is in concordance with the behavior of N_9 in Fig. 2.3 in the sense that the polygonal number grows as the revolution frequency decreases.

In Fig. 2.8 the acceleration level settles within the vicinity of 4 m/s^2. A long-term vibration cycle can also be identified. The vibration amplitude does not grow infinitely because increasing vibration causes the nip to widen, which leads to higher cover stiffness, limiting the growth of the vibration amplitude. Increased vibration levels may also affect the self-excited vibration mechanism if the natural frequencies of the system alter significantly due to changing cover stiffness, that is, the deformation pattern may not lock into a particular polygonal shape.

On the other hand, it was observed that an increasing vibration amplitude leads to growing cover temperature. This lowers the cover stiffness in the nip, possibly creating another non-resonance condition. Consequently, under such condition, the vibration amplitude and cover temperature begin to fall creating opposite changes in the cover stiffness, thus increasing the amplitude and temperature again. Therefore, the long-term vibration cycle may be seen as a consequence of complicated coupled thermal-mechanical behavior of the polymer cover.

In conclusion, nonlinear and non–isothermal phenomena start to arise only at high vibration amplitudes. Therefore, the studied 1D model can be used to describe the onset of the self-excited vibration mechanism and the loss of stability and small amplitude vibrations of the system in a physically logical, qualitative manner. The 2D FE approach can be easily extended to include the thermal behavior of the polymer cover to study the impact of cover temperature on the overall system behavior.

3. Traveling waves

At high speeds, industrial rolling contact machinery can be rendered inoperable by traveling waves, which arise from a nip and stretch out to the circumference of the polymer cover of a cylinder, see Fig. 3.1. Generally speaking, traveling waves begin to take shape when the minimum wave speed in a polymer cover is reached under rolling contact. Therefore, traveling waves appear especially in polyurethane and other rubber-like covers because of their low elastic moduli and, consequently, low characteristic wave speeds.

The traveling waves have undesirable effects on polymer covers. Again, let us consider a two-cylinder machine with a polymer cover on the other cylinder. Waves traveling in the cover generate heat, which in turn hastens the failure of the cover. On the other hand, the waving increases the rolling resistance of the cover so that more power is required to keep the machine running at a certain speed. In addition, waves in the nip may have an effect on the vibration of the cylinders.

In the following, traveling waves in a cylinder cover are studied. By understanding the underlying physical mechanisms, a coherent overall picture of the phenomenon will be given.

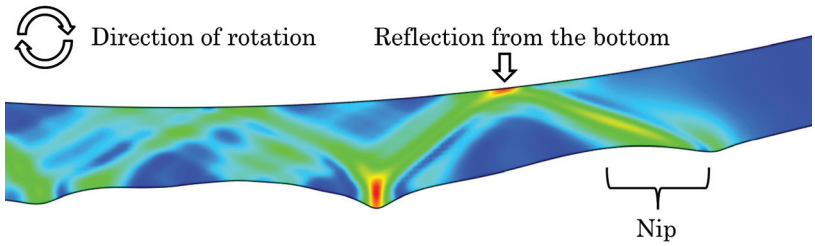

Figure 3.1. Simulated contact-induced traveling wave in a polymeric cylinder cover from a 2D FE model. The contour depicts the von Mises stress distribution in the cover, red stands for high stress and dark blue tends towards zero stress.

3.1 Overview of literature

The study of cylinder cover dynamics constitutes a 2D plane strain problem where typically a relatively long hard cylinder with a thin soft cover is rolling in contact with another cylinder. The plane strain feature establishes a fundamental difference between covered cylinders and, for example, vehicle tires which often have been studied by using ring or shell models, for example, see the papers by Soedel (1975) and Padovan (1975, 1976). In other words, the traveling waves in cylinder covers should not be viewed too closely in terms of other circular structures.

Nowadays, there is a large number of readily available computational methods, which could be used to study contact-induced traveling waves in thin cylinder covers, for example, see the papers by Oden and Lin (1986); Padovan (1987); Zehil and Gavin (2013, 2014). However, only a few works, analytical or computational, that have significant relevance to the detailed study of traveling waves in thin cylinder covers can be found. In their elaborate mathematical study of the steady-state motion of a spinning cylinder, Rabier and Oden (1989) noted a close relationship between waves in the cylinder and Rayleigh waves propagating in an elastic half-space, but the matter was not studied to a larger extent. However, this observation will turn out to be helpful in the case of traveling waves in thin cylinder covers. Chatterjee et al. (1999) used a Pasternak-type foundation model to study waves in rotating tires by formulating a non-linear boundary value contact problem associated with steady-state rolling conditions. Their foundation model, unlike a typical ring model for a tire, does not include stiffness associated with bending. Therefore, we find that such a model is suitable for the study of cylinder cover dynamics. In a recent paper, Qiu (2009) developed a 2D semianalytical plane strain model for a covered cylinder rolling in contact with a rigid surface. He calculated the natural frequency spectrum for the covered cylinder and used the frequencies to estimate the critical rolling speed at which traveling waves start to emerge in a cover.

In order to understand the nature of the traveling wave phenomenon to a deeper extent, we use a 2D plane strain FE model to study a polymer-covered cylinder rolling in contact with another cylinder through numerical experiments. For analytical study, we utilize a 1D Pasternak-type foundation model, which catches the essentials of the traveling wave phenomenon in the cylinder cover.

3.2 2D numerical experimentation

The system under investigation consists of a steel cylinder and a cylinder with a radius of $R = 0.21$ m including a 6 mm thick polymer cover attached to a steel core (see Fig. 3.2). The steel parts are modeled as rigid and the polymer as a linear isotropic viscoelastic material. In the utilized reference frame fixed to the viscoelastically covered cylinder, the other cylinder moves in rolling contact around the covered cylinder which in this frame appears to be at rest. This approach saves a lot of computation time. Because the covered cylinder is modeled as stationary, the Coriolis and centrifugal forces acting on the cover due to rotation are not intrinsically accounted for. However, these forces would have little effect on the cover dynamics if they were to be taken into account (PIII, PIV).

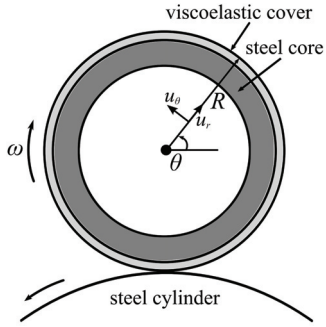

Figure 3.2. 2D rolling contact system with a polymer cover on the other cylinder.

A total of 86680 linear isoparametric quadrilateral plane strain finite elements with a characteristic element size of 0.3 mm are used to model the cover. The contact between the cylinders is frictionless. The eigenmodes of the cover are computed using the Lanczos method and in dynamic simulations an explicit time integration scheme is employed. All modeling and calculations are done using Abaqus 6.10 FE software.

Fig. 3.3 shows two different mode families of the polymer cover. The dark color stands for positive and white for negative radial displacements. In each mode family, every individual mode possesses an integer number of waves on the cylinder circumference. For the shown modes the number of waves is one hundred, thus the *principal mode number* in both cases is N = 100. For the primary mode in Fig. 3.3a the radial displacement does not change sign along an initially straight radial line from the bottom to the surface of the polymer cover. For the secondary mode I in Fig. 3.3b, the sign changes once in the radial direction. For the secondary mode II

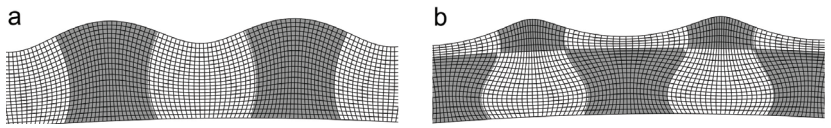

Figure 3.3. Two mode families. The dark and white areas represent positive and negative radial displacements, respectively. a) Primary mode, f_{100} = 5016 Hz, b) Secondary mode I, f_{100} = 8296 Hz.

the sign changes twice and so on. Due to the finite thickness of the cover layer, there is an infinite number of higher mode families, each of which corresponds to a secondary mode number.

The natural frequencies of three mode families as a function of the principal mode number N are shown in Fig. 3.4. The lowest primary mode appears at 2200 Hz and the lowest secondary modes I and II at 6700 Hz and 11200 Hz, respectively. At higher mode numbers, the illustrated curves display almost constant slopes.

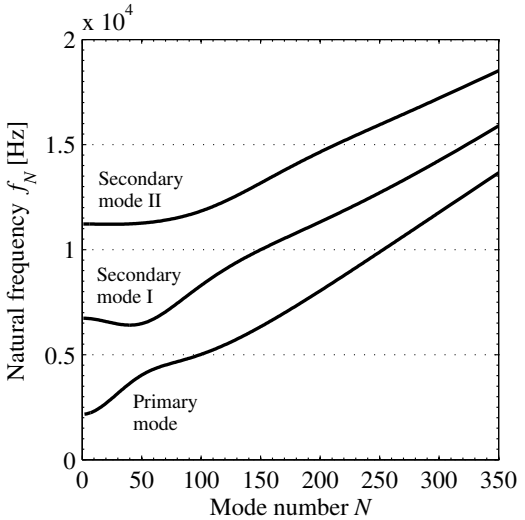

Figure 3.4. Natural frequencies for the primary modes and secondary modes I and II of the polymer cover as a function of the principal mode number N.

If a contact load travels over one full wave of an eigenmode having the wavelength λ_N in the same time it takes for the eigenmode to go through one oscillation, that eigenmode will go into resonance. The time to travel over one wavelength is $T = \frac{\lambda_N}{\omega R} = \frac{2\pi}{N\omega} = \frac{1}{Nf}$, where $f = \frac{\omega}{2\pi}$ is the rotational frequency of the load. On the other hand, the period of oscillation of the mode is $T = \frac{2\pi}{\omega_N} = \frac{1}{f_N}$. From the foregoing, we obtain the resonance condition, cf. (Soedel, 1975),

$$\omega = \frac{\omega_N}{N} \qquad \text{or} \qquad f = \frac{f_N}{N} \,. \tag{3.1}$$

If a radial point-like harmonic load with a driving frequency corresponding to a particular natural frequency f_N is exerted on the polymer cover at a fixed position, it generates a modified Rayleigh wave, which propagates along the circumference of the cover. The wave is said to be *modified* due to the fact that the cover has a finite thickness. The wavelength of the traveling wave equals the wavelength of the eigenmode related to the excited natural frequency.

Let us consider a modified Rayleigh wave with a wavelength of $2\pi R/N$. The frequency of this wave equals the natural frequency f_N of the Nth eigenmode. Therefore, the phase velocity of this Rayleigh wave is

$$v_p = \frac{2\pi R}{N} f_N = 2\pi R \frac{f_N}{N} \qquad \text{or} \qquad \frac{v_p}{2\pi R} = \frac{f_N}{N} = f \ , \tag{3.2}$$

where f is the rotational frequency of the load which resonates with the Nth eigenmode of the cover. The computed values of f_N/N as a function of the principal mode number N are presented for three mode families in Fig. 3.5. In the figure, the curve of the primary modes approaches a constant value around 39 Hz at higher modes, indicating that there is a cutoff rotational frequency, or a critical speed (51.5 m/s), under which the resonance condition is not fulfilled by any mode. On the other hand, one can see that also the phase velocity of the modified Rayleigh waves approaches a constant value at higher frequencies. This means that the high frequency waves with short wavelengths in the cover layer become non-dispersive, as is the case for Rayleigh waves over a half-space.

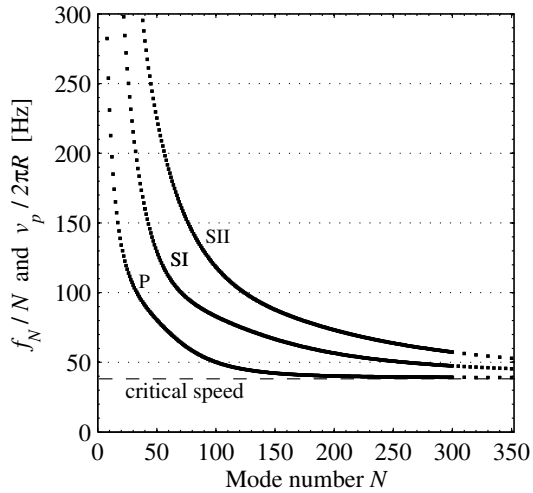

Figure 3.5. Natural frequencies divided by the principal mode number for the primary and two secondary modes and equivalently the Rayleigh wave phase velocity.

Considering the eigenmode-based resonance approach in conjunction with the eigenmode expansion of the modified Rayleigh wave leads us to the conclusion that the traveling waves cannot exist in the subcritical region because all the natural modes in the eigenmode expansion of the wave are subcritically excited. The modes have small phase lags with respect to the load leading to a quasistatic, that is, local and non-propagating disturbance. This implies that the critical speed is also the minimum phase velocity of the modified Rayleigh waves in the polymer cover.

Figs. 3.6a and 3.6b present the deformed shapes of the polymer cover and the von Mises stresses at the rotational frequencies $f = 50.16$ and 80.5 Hz, chosen according to the primary modes $N = 100$ and 50, respectively. In Fig. 3.6a the primary eigenmode can be clearly seen to be dominant in the traveling wave. At the higher rotational frequency $f =$ 80.5 Hz in Fig. 3.6b, the traveling wave has a more irregular shape. Wave formations with reflections from the rigid bottom under the polymer cover are clearly displayed in Fig. 3.6b.

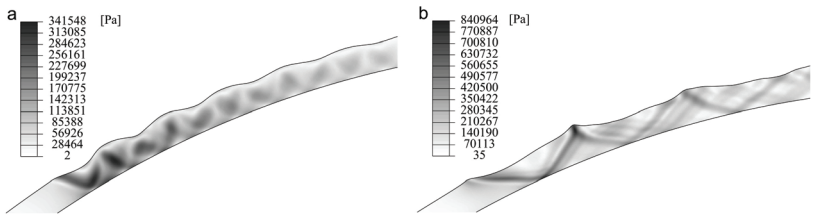

Figure 3.6. Deformed shape of the polymer cover with the von Mises stress contour [Pa] at the rotational frequencies a) $f = 50.16$ Hz and b) $f = 80.5$ Hz.

In both cases ($f = 50.16$ and 80.5 Hz), a single surface node on the polymer cover is chosen and a frequency spectrum is calculated by the Fast Fourier Transform (FFT) from the radial displacement of the node after the node has oscillated freely outside the nip for a short time interval during which the waves have passed the node. For both cases in Fig. 3.7, the frequency values of the amplitude peaks coincide with the natural frequencies for the primary mode family and the secondary mode families with a relative error of less than 1 %. It can be concluded that Fig. 3.7 gives the modal decomposition (without phase information) of the traveling waves, and the peaks correspond to the resonating modes according to Eq. (3.1). The amplitude peaks corresponding to the primary mode family are clearly the highest in Fig. 3.7. The other amplitude peaks are related to the higher mode families. Therefore, Fig. 3.7 indicates that the

higher mode family curves, if plotted in Fig. 3.5, would also approach the asymptotic and almost horizontal primary mode family curve of Fig. 3.5. Thus, for rotational frequencies approaching the critical speed $f = 39$ Hz, a large number of tightly packed modes fulfill the resonance condition of Eq. (3.1) simultaneously.

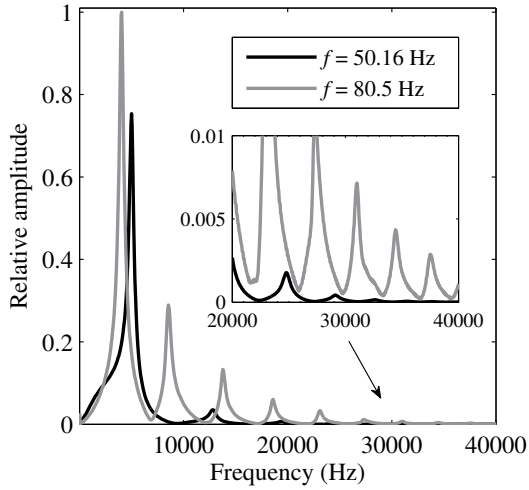

Figure 3.7. Frequency spectrum calculated by FFT from the radial displacement of a single surface node executing free oscillations for $f = 50.16$ and 80.5 Hz.

In addition, it should be noted that each amplitude peak has a certain width in Fig. 3.7 which indicates that instead of a single natural mode from each family being active, a large number of modes are activated. This is a manifestation of the fact that a modified Rayleigh wave corresponding to a certain mode family is a superposition of the modes in that family. Such waves arising from the different mode families combine into the wave which we refer to as the *traveling wave*.

Finally, we note the pioneering work of Goldstein (1965), in which he showed that if the velocity of a semi-infinite uniform loading on an elastic half-space equals the velocity of the Rayleigh wave for the medium, a so-called Rayleigh wave resonance takes place. When this happens, the Rayleigh waves arising at the front end of the load will have a common front, which moves together with the load. Thus, in the neighborhood of the front end of the load, a superposition of Rayleigh waves with the same phase occurs. In conclusion, we find that the traveling wave phenomenon at hand is best described as a *Rayleigh wave resonance* in which contact-induced modified Rayleigh waves arising in the nip at critical and supercritical speeds superpose to form a traveling wave.

3.3 1D cover model

The 1D analytical model studied in this section consists of a non-rotating rigid cylinder with a cover subjected to a moving radial point load P (see Fig. 3.8). In reality, the load would be a distributed one, but since the contact area, the nip, is typically small in rolling contact machines, it is reasonable to present the load resultant as a point force acting at the load center. The cover is modeled as a Pasternak-type foundation consisting of a shear layer attached to a Kelvin-Voigt assembly.

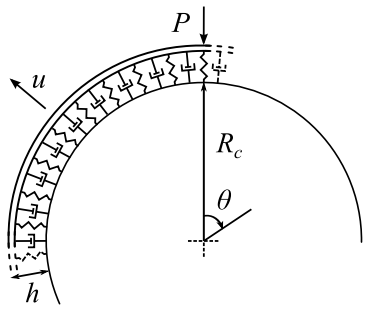

Figure 3.8. 1D Analytical model for a covered cylinder subjected to circumferentially moving point load P.

The equation of motion in a coordinate system fixed to the cylinder in terms of the radial displacement u of the shear layer reads

$$u_{tt} + \frac{E}{\rho h^2}u + \frac{\alpha}{\rho h^2}u_t - \frac{\kappa G}{\rho R^2}u_{\theta\theta} - \frac{\kappa\beta}{\rho R^2}u_{\theta\theta t} = P(\theta, t)\ . \tag{3.3}$$

Above, E is the Young's modulus and G is the shear modulus of the cover, and α and β are the corresponding strain rate damping parameters, respectively. The density and thickness of the cover are ρ and h, respectively. The radius $R = R_c + h/2$ is used to determine the effective width of a material element. In addition, we introduce a shape factor κ for the shear layer, which accounts for the total shear force on the cover layer cross-section. For a moving constant point load, we have $P(\theta, t) = P_0\delta(\theta - \Omega t)$, where P_0 is the load amplitude and Ω is the angular velocity of the load. The rotational frequency of the load is $f_{\text{rot}} = \Omega/2\pi$. Note that the term containing $u_{\theta\theta}$ in Eq. (3.3) stems from the Pasternak foundation model and is typical for all shear layer models. This term couples the adjacent material elements to each other. The model description is completed by the requirement of continuity of the displacement and slope which leads to

$$u(0, t) = u(2\pi, t) \quad \text{and} \quad u_\theta(0, t) = u_\theta(2\pi, t)\ . \tag{3.4}$$

Each natural mode, $\sin(n\theta)$ or $\cos(n\theta)$, of the free undamped cover consists of n full waves on the cover circumference, with the exception of $n = 0$, which is the breathing mode. As n increases, the wavelength in a mode decreases. The solution for the moving load problem can be expanded in terms of the natural modes leading to

$$u(\theta, t) = \sum_{n=1}^{\infty} \left[c_n(t) \sin(n\theta) + d_n(t) \cos(n\theta) \right] + d_0(t) \; . \tag{3.5}$$

By substituting Eq. (3.5) into Eq. (3.3), differential equations for the modal expansion coefficients c_n, d_n and d_0 follow, from which they can be solved. The steady-state vibration response can be shown to be

$$u(\theta, t) = \sum_{n=1}^{\infty} A_n \cos\left[n(\Omega t - \theta) - \phi_n \right] + \frac{P_0}{2\pi\omega_0^2} \; . \tag{3.6}$$

The amplitudes A_n and the phase shifts ϕ_n are calculated from the expressions

$$A_n = \frac{P_0}{\pi \sqrt{\left[\omega_n^2 - (n\Omega)^2\right]^2 + (2\zeta_n \omega_n n\Omega)^2}} \; , \tag{3.7}$$

$$\tan\phi_n = \frac{2\zeta_n \omega_n n\Omega}{\omega_n^2 - (n\Omega)^2} \quad , \quad 0 \leq \phi_n < \pi \quad (n = 1, 2, \ldots) \; , \tag{3.8}$$

where the natural angular frequencies and modal damping ratios are given, respectively, by $(n = 0, 1, 2, \ldots)$

$$\omega_n = \sqrt{\frac{1}{\rho} \left(\frac{E}{h^2} + \frac{\kappa G}{R^2} n^2 \right)} \; , \tag{3.9}$$

$$\zeta_n = \frac{\alpha/h^2 + \kappa\beta n^2/R^2}{2\rho\omega_n} \; . \tag{3.10}$$

At this point, we compare the 1D elastic cover model to a 2D FE model. In Fig. 3.9, the undamped natural frequencies $f_n = \omega_n/2\pi$ of the 1D model calculated from Eq. (3.9) for two different cover thicknesses are compared to those given by the 2D plane strain FE model. The same parameter values are used for both models, apart from the shape factor κ present only in the analytical model and obtained by adjusting the analytical 1D results to those calculated from the 2D FE model. With the shape factor $\kappa = 6/7$, we find a good agreement between the two different models, especially at higher natural modes. For $n = 100$, the calculated natural frequencies for the 1D and 2D models are 4146 and 4147 Hz, respectively. The correspondence between the models is good and the mode shapes also coincide (PIV). The differences in the natural frequencies between the two models at the lower modes in Fig. 3.9 are due to the dissimilar throughout-thickness behavior of the two cover models. The 2D model captures the

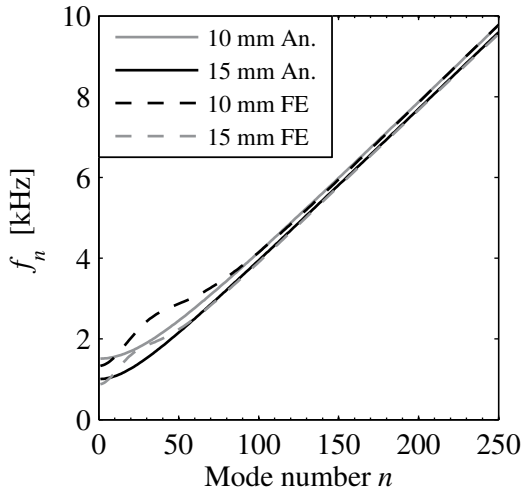

Figure 3.9. Undamped natural frequencies of both the 1D analytical cover model (solid lines) and the 2D FE model (dashed lines) for thicknesses of 10 and 15 mm.

dispersive wave characteristics of the cylinder cover in a more detailed manner, especially in the case of lower modes, since these modes penetrate deeper into the cover and interact with the bottom of the cover layer. However, the higher modes are of primary interest in the study of the traveling waves, mainly due to the fact that they appear at lower load speeds and indicate the speed range of the system within which the traveling waves first start to appear.

On the basis of the comparison, we find that the 1D model captures the essential features of the 2D cylinder cover problem. The reason for studying the 1D analytical model is that it yields useful explicit expressions for some important features of the traveling wave phenomenon unlike the performed 2D numerical experiment. An additional benefit is that the 1D model is three orders of magnitude faster in simulations than the 2D FE model. It can be seen from Eq. (3.7) that without damping the nth mode is in resonance when $\omega_n = n\Omega$. Therefore, the resonant angular velocity Ω_n of the load for each mode is given by

$$\Omega_n = \frac{\omega_n}{n} = \sqrt{\frac{1}{\rho}\left(\frac{E}{n^2h^2} + \frac{\kappa G}{R^2}\right)}\,, \tag{3.11}$$

which is of the same form ($\Omega_n = \omega_n/n$) as used, *ad hoc*, in the 2D FE case. The lowest resonant speed is achieved in the limit $n \to \infty$, which leads to the critical angular speed of the system

$$\Omega_{\text{cr}} = \sqrt{\frac{\kappa G}{\rho R^2}}\,. \tag{3.12}$$

In terms of tangential load velocity on the cover surface, the critical speed in the undamped case is

$$v_{\mathrm{cr}} = \hat{R}\sqrt{\frac{\kappa G}{\rho R^2}}\,, \tag{3.13}$$

where $\hat{R} = R_c + h$. It can be seen from Eq. (3.13) that the critical speed is independent of the Young's modulus of the cover. Note that the critical angular speed is an accumulation point of the angular velocities Ω_n for $n \to \infty$. Therefore, at the critical speed, a large number of natural modes are in resonance or very close to it simultaneously.

To further elucidate the dynamic behavior of the system, the dispersion relation for traveling waves in the shear layer is obtained from Eq. (3.3) by a solution of the form $u = \mathrm{e}^{\mathrm{i}(k\hat{R}\theta - \omega t)}$, which leads to

$$\omega(k) = \pm\sqrt{\frac{1}{\rho}\left(\frac{E}{h^2} + \frac{\kappa G}{R^2}\hat{R}^2k^2\right)}\,, \tag{3.14}$$

where $k = 2\pi/\lambda$ is the wavenumber. The phase velocity is defined as $v = \omega/k$. Thus, in the small wavelength limit $k \to \infty$, Eq. (3.14) yields for the minimum phase velocity the expression

$$v_{\mathrm{min}} = \hat{R}\sqrt{\frac{\kappa G}{\rho R^2}} \equiv v_{\mathrm{cr}}\,. \tag{3.15}$$

Therefore, the critical speed based on the resonance condition equals the minimum phase velocity of the waves in the shear layer.

To form a standing wave vibration mode in the cover from two identical waves traveling in opposite directions, the wavenumber must satisfy $k = n/\hat{R}$, that is, the cylinder circumference must be divisible by the wavelength $\lambda_n = 2\pi\hat{R}/n$ of the wave. In this case, the discrete dispersion relation and wave propagation velocity of a traveling wave are given by

$$\omega(n) = \pm\sqrt{\frac{1}{\rho}\left(\frac{E}{h^2} + \frac{\kappa G}{R^2}n^2\right)}\,, \tag{3.16}$$

$$v(n) = \pm\hat{R}\sqrt{\frac{1}{\rho}\left(\frac{E}{n^2h^2} + \frac{\kappa G}{R^2}\right)}\,, \tag{3.17}$$

respectively. It can be seen that Eq. (3.17) describes how the wave velocity increases due to wave dispersion at lower values of n. We can conclude that when a vibration resonance due to the moving point load takes place in the cylinder cover, from a different point of view, a traveling wave arises in the cylinder cover as a result of the superposition of waves, similarly to the Rayleigh wave resonance discussed earlier on the basis of 2D numerical experiments.

The 1D cover model can be modified for industrial purposes by changing the material model from elastic to viscoelastic. The solution to the modified frequency-dependent viscoelastic equation of motion is still given by the modal expansion (3.5). In more detail, the cover becomes viscoelastic by setting the strain rate damping parameters α and β to zero in Eq. (3.3) and by replacing the moduli by complex moduli, that is,

$$E \rightarrow E^* = E_s + \mathrm{j}E_l \quad \text{and} \quad G \rightarrow G^* = G_s + \mathrm{j}G_l \ . \tag{3.18}$$

The frequency-dependency of the viscoelastic polymer cover is accounted for through the generalized Maxwell model. With this model, the tension-compression storage and loss moduli are calculated for each mode by

$$E_s(n\Omega) = E_\infty + \sum_{i=1}^{m} E_i \frac{(n\Omega\tau_i)^2}{1+(n\Omega\tau_i)^2} \ , \tag{3.19}$$

$$E_l(n\Omega) = \sum_{i=1}^{m} E_i \frac{n\Omega\tau_i}{1+(n\Omega\tau_i)^2} \ , \tag{3.20}$$

respectively. For an incompressible rubber-like polymer the shear storage and loss moduli are given by $G_s(n\Omega) = E_s(n\Omega)/3$, $G_l(n\Omega) = E_l(n\Omega)/3$. The stiffness of the polymer begins to increase due to the transition from the rubber plateau towards the stiffer glass region of the polymer at high frequencies. With the parameter values used for the 2D FE model this stiffening did not occur to notable extent. However, in the next section computations are performed using the viscoelastic version of the 1D model and a wider relaxation spectrum, see Fig. 3.10, is used for the 1D cover model than for the 2D model and the effect of stiffening becomes evident.

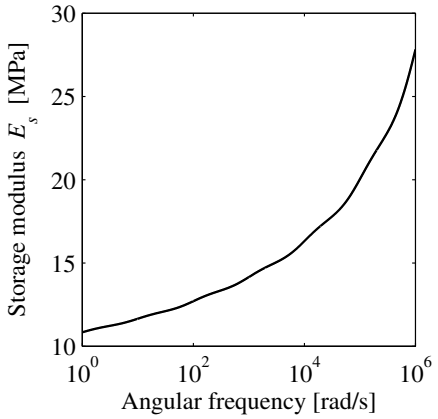

Figure 3.10. Storage modulus E_s of the utilized viscoelastic material under harmonic excitation. The material is incompressible and, thus, the Poisson ratio has the value of 0.5.

3.4 1D simulation results

Let us study the case of a moving constant point load. Fig. 3.11 shows the viscoelastic modal phase shifts as a function of the rotational frequency of the moving load and the mode number n. The resonant rotational frequencies $f_{\mathrm{rot},n} = f_n/n$ and the locations of the maximums of the modal amplitudes, as a function of n have been added as continuous curves into the figure. The 90-degree-curve for the modal phase shifts is marked by the same line as $f_{\mathrm{rot},n}$. When the modal phase shifts approach the resonance value of 90 degrees, the displacements localized in the vicinity of the load become increasingly asymmetric with respect to the load. The lowest rotational frequency values for the curve $f_{\mathrm{rot},n}$ is attained by the mode $n = 182$, according to which the critical speed is $f = 39.82$ Hz. The curves rise at higher modes due to the stiffening of the viscoelastic material caused by increasing vibration frequencies.

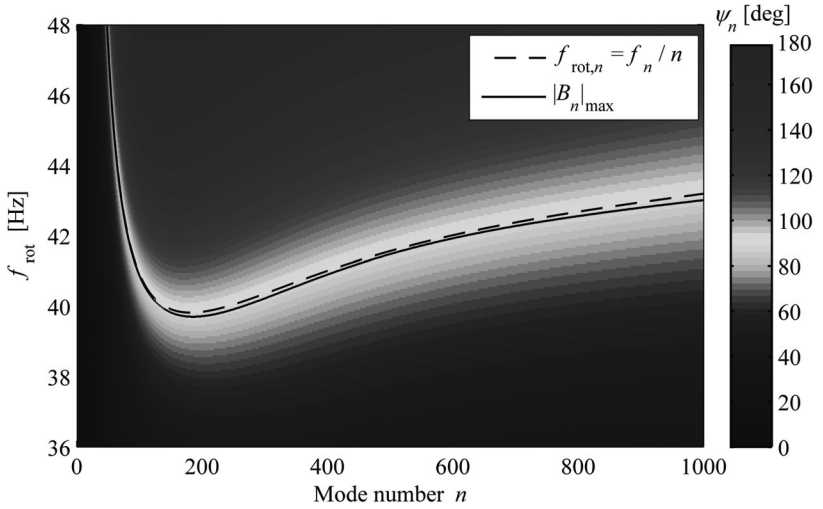

Figure 3.11. Viscoelastic modal phase shifts ψ_n, the resonant rotational frequency curve $f_{\mathrm{rot},n} = f_n/n$ and the locations of the maximums of the modal amplitudes $|B_n|_{\max}$. Below the dashed line the modal phase shifts are smaller than $90°$.

The steady-state response of the viscoelastic cylinder cover for the rotational frequency range 1–100 Hz of the moving point load is shown in Fig. 3.12. We may conclude that although the determination of an exact critical speed in a real (damped) case may be difficult, the resonance interpretation is still a proper backbone for the traveling wave phenomenon and gives a good estimate for the location of the critical speed range of the system ($f \approx 39$–40 Hz) within which the cover response shifts from a local quasi-static deformation to a non-local traveling wave. Further

development of the viscoelastic cover model in terms of multiple moving point and distributed loads will be carried out in future work (Karttunen and von Hertzen, 2015).

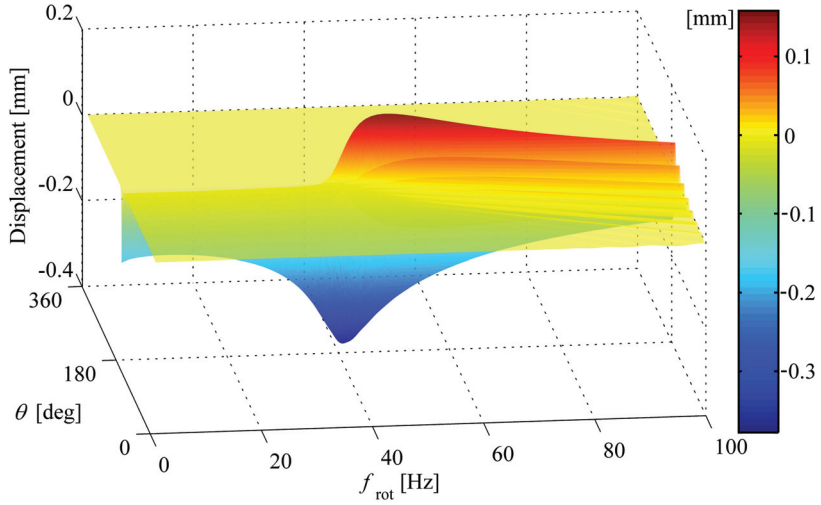

Figure 3.12. Steady-state response of the viscoelastic cylinder cover for the rotational frequency range 1–100 Hz of the moving point load. The point load is located at $\theta = 180°$ and the area in front of the load at $\theta > 180°$.

4. Summary

In this thesis, the goal was to provide thorough explanations of the self-excited vibration mechanism and the traveling wave phenomenon, which take place in a two-cylinder rolling contact machine with a polymer cover on the other cylinder. The focus was on analytical and computational modeling of the phenomena.

The self-excited vibration mechanism was first studied using a 1D analytical model for a two-cylinder system in which the viscoelastic properties of the cover on the other cylinder were accounted for by the standard linear solid model. The equations of motion for the model constituted a set of delay differential equations, which were analyzed through numerical stability analysis. It was found that the self-excited vibration mechanism is active when the frequency of the cover deformation induced excitation is close to the eigenfrequency of the system, which corresponds to the eigenmode in which the cylinders are vibrating in opposite phases. The vibrations are strongest when the phase of the residual deformation of the cover leads the phase of the nip gap between the cylinders by 90 degrees.

Next, a 2D FE model was developed for a two-cylinder system and realistic cover deformation patterns due to the self-excited vibrations were obtained through numerical simulations. The results from the 1D and 2D models were found to be in good agreement. Finally, empirical information was obtained on the phenomenon by performing an experiment with an industrial rolling contact machine. It was concluded that non-linear and non-isothermal phenomena start to arise only at high vibration amplitudes. Therefore, the physical explanation given by the 1D analytical model for the self-excited vibration mechanism was found to be reliable and the model can be used to describe the onset of the phenomenon and the small amplitude vibrations in a two-cylinder system.

As for the traveling waves in a polymer cover of a cylinder, a 2D plane strain FE model was first used to perform numerical experiments in order to obtain an overall picture of the phenomenon. The 2D results from the eigenmode analysis of the cover showed that an infinite number of natural mode families exist for the cylinder cover due to its finite thickness. A critical speed below which the traveling waves did not appear was calculated on the basis of a resonance condition using the modal information. The critical speed was found to be an accumulation point at which a large number of natural modes fulfill the resonance condition simultaneously. In dynamic rolling contact simulations, the waves were identified as modified Rayleigh waves. Ultimately, it was found that the traveling wave phenomenon is best described as a Rayleigh wave resonance in which contact-induced modified Rayleigh waves, representing different mode families, arise in the nip at critical and supercritical rolling speeds and the waves superpose to form a strong traveling wave.

After studying the traveling waves through the 2D FE numerical experimentation, a 1D analytical cover model was developed for an elastic cylinder cover with damping. Finally, the 1D cover model was developed further by describing the cover material as a frequency-dependent viscoelastic polymer. By performing a comparison between the natural frequencies and mode shapes calculated from both the analytical 1D model and the 2D FE model, it was found that the 1D analytical model captures the essential features of the traveling wave phenomenon, and can be used for a detailed study of the waves. The 1D model is up to thousand times faster in simulations than the 2D FE model. Simulation results from the 1D cover model showed that the determination of an exact critical speed may be difficult if the cover includes damping. However, the resonance interpretation for the phenomenon still gives a good estimate for the critical speed range within which the cover response shifts from a local quasi-static deformation to a non-local traveling wave. A wide relaxation spectrum can be easily included in the viscoelastic version of the 1D model and, thus, the model offers a practical and fast tool for calculating estimates for the critical speeds of polymer covers in industrial use. It is reasonable to design the covers so that the traveling waves will never appear.

Bibliography

Chatterjee, A., Cusumano, J., Zolock, J., 1999. On contact-induced standing waves in rotating tyres: Experiment and theory. *Journal of Sound and Vibration* 227 (5), 1049–1081.

Chinn, F., 1999. Dynamic instability of poly covered press rolls. *Pulp & Paper Canada* 100 (1), 11–14.

Goldstein, R., 1965. Rayleigh waves and resonance phenomena in elastic bodies. *Journal of Applied Mathematics and Mechanics* 29 (3), 608–619.

Järvenpää, V.-M., Yuan, L., 2007. Numerical modeling of paper machine roll contact with regenerative out-of-roundness excitation. In: *IUTAM Symposium on Multiscale Problems in Multibody System Contacts*. pp. 55–64.

Järvenpää, V.-M., Yuan, L., 2009. Active vibration control of multibody rolling contact system. In: *Motion and Vibration Control*. pp. 155–164.

Jorkama, M., von Hertzen, R., 2003. Delay phenomena in roll vibrations. In: *Proceedings of the VIII Finnish Mechanics Days*. pp. 111–121.

Jorkama, M., von Hertzen, R., 2007. Two-drum winder stability analysis. *Pulp & Paper Canada* 108 (5), 35–37.

Karttunen, A. T., von Hertzen, R., 2015. Steady-state vibration of a viscoelastic cylinder cover subjected to moving loads. *European Journal of Mechanics — A/Solids* (Revised manuscript under review).

METLA, 2014. *Forest industries and labour*.
URL `http://www.metla.fi/metla/finland/finland-forest-industries.htm`

Oden, J., Lin, T., 1986. The general rolling-contact problem for finite deformations of a viscoelastic cylinder. *Computer Methods in Applied Mechanics and Engineering* 57 (3), 297–367.

Padovan, J., 1975. Traveling waves vibrations and buckling of rotating anisotropic shells of revolution by finite elements. *International Journal of Solids and Structures* 11 (12), 1367–1380.

Padovan, J., 1976. On viscoelasticity and standing waves in tires. *Tire Science and Technology* 4 (4), 233–246.

Padovan, J., 1987. Finite-element analysis of steady and transiently rolling nonlinear viscoelastic structure, 1. theory. *Computers & Structures* 27 (2), 249–257.

Qiu, X., 2009. Full two-dimensional model for rolling resistance. II: Viscoelastic cylinders on rigid ground. *Journal of Engineering Mechanics* 135 (1), 20–30.

Rabier, P., Oden, J., 1989. *Bifurcation in rotating bodies*. Springer-Verlag.

Rautiainen, H., Koriseva, J., Stapels, R., 2000. New vibration analysis tools optimize multi-nip calender operation. *Pulp & Paper Canada* 101 (6), 151–154.

Soedel, W., 1975. On the dynamic response of rolling tires according to thin shell approximations. *Journal of Sound and Vibration* 41 (2), 233–246.

Sowa, N., Kondou, T., Mori, H., Choi, M., 2006. Method of preventing unstable vibration caused by time delays in contact rotating systems (application of new stability analysis). *JSME International Journal, Series C* 49 (4), 973–982.

Sueoka, A., Ryu, T., Kondou, T., Tsuda, Y., Katayama, K., Takasaki, K., Yamaguchi, M., Hirooka, H., 1996. Polygonal deformation of roll-covering rubber. *JSME International Journal, Series C* 39 (1), 1–10.

Sueoka, A., Ryu, T., Yoshikawa, M., Kondou, T., Tsuda, Y., 1998. Pattern formation generated in a winder system of textile machine. *JSME International Journal, Series C* 41 (3), 630–638.

Vuoristo, T., 2004. *Effect of strain rate on the deformation behavior of dual phase steels and particle reinforced polymer composites*. Ph.D. thesis, Tampere University of Technology.

Vuoristo, T., Kuokkala, V.-T., 2002. Creep, recovery and high strain rate response of soft roll cover materials. *Mechanics of Materials* 34 (8), 493–504.

Vuoristo, T., Kuokkala, V.-T., 2004. Effect of strain rate, moisture and temperature on the deformation behavior of polymer roll covers. *Experimental Mechanics* 44 (3), 313–319.

Vuoristo, T., Kuokkala, V.-T., Keskinen, E., 2000. Dynamic compression testing of particle-reinforced polymer roll cover materials. *Composites: Part A* 31 (8), 815–822.

Vuoristo, T., Kuokkala, V.-T., Keskinen, E., 2002. Modeling of the deformation behavior of polymer composites at high strain rates and at elevated temperatures. *Key Engineering Materials* 221–222, 221–232.

Ward, I., Sweeney, J., 2004. *An Introduction to the Mechanical Properties of Solid Polymers*. John Wiley & Sons Ltd.

Yuan, L., 2002. *Analysis of delay phenomena in roll dynamics*. Ph.D. thesis, Tampere University of Technology.

Yuan, L., Järvenpää, V.-M., 2009. Nonlinear vibrations in a covered roll system with viscoelastic contact. *Communications in Nonlinear Science and Numerical Simulation* 14 (7), 3170–3178.

Zehil, G.-P., Gavin, H., 2013. Three-dimensional boundary element formulation of an incompressible viscoelastic layer of finite thickness applied to the rolling resistance of a rigid sphere. *International Journal of Solids and Structures* 50 (6), 833–842.

Zehil, G.-P., Gavin, H., 2014. Rolling resistance of a rigid sphere with viscoelastic coatings. *International Journal of Solids and Structures* 51 (3–4), 822—838.

The development of polymeric cylinder covers has been rapid since the 1990s and their use in paper machines has become commonplace

In contrast to their many virtues, the polymer covers also induce and suffer from detrimental dynamic phenomena, which have not been fully explained yet, let alone dealt with. Two prime examples of such phenomena are: 1) the self-excited vibration mechanism, barring, which is caused by viscoelastic cover deformations acting as time-delayed feedbacks in a rolling contact machine, and 2) a contact-induced traveling wave phenomenon occuring in a cover at high rolling speeds. These two are the subject of this dissertation.

Aalto-DD 179/2015

ISBN 978-952-60-6501-4 (printed)
ISBN 978-952-60-6502-1 (pdf)
ISSN-L 1799-4934
ISSN 1799-4934 (printed)
ISSN 1799-4942 (pdf)

Aalto University
School of Engineering
Department of Applied Mechanics
www.aalto.fi

BUSINESS + ECONOMY

ART + DESIGN + ARCHITECTURE

SCIENCE + TECHNOLOGY

CROSSOVER

DOCTORAL DISSERTATIONS